Journal of Renewable Energy and Environment

Research Article

Journal Homepage: www.jree.ir

Experimental Investigation of the Thermal Performance of Vacuum Tube Solar Collectors (VTSC) Using Alumina Nanofluids

Seyed Amir Hossein Zamzamian, Mohsen Mansouri*

Solar Energy Group, Department of Energy, Materials and Energy Research Center (MERC), Karaj, Iran.

PAPER INFO

Paper history:
Received 04 March 2019
Accepted in revised form 29 March 2019

Keywords:
Nanofluid
Thermal Performance
Vacuum Tube
Solar Collector
Thermal Conductivity

ABSTRACT

The enhancement of the thermal performance of Vacuum Tube Solar Collectors (VTSC) was studied by using alumina nanofluid as working fluid. VTSC is a simple and commonly utilized type of collector. This study established the heat transfer experimental model of all glass VTSCs used in a forced-circulation solar water heating system using alumina nanofluid as base fluid. Al_2O_3 (with an average particle size of 15 nm) nanoparticles were provided and utilized to prepare nanofluids at a low mass concentration (0.5–1 wt. %). The thermal performances of VTSC were 15.3 %, 25.7 %, and 27.2 % for the deionized water and Al_2O_3/water nanofluids with 0.5 and 1.0 wt. % as the working fluid, respectively. Generally, for Al_2O_3/water nanofluids with mass concentrations of 0.5 and 1.0 wt. %, the thermal performance increased by 67.9 % and 77.7 %, respectively, superior to that of vacuum tube using deionized water as the working fluid. Experimental results also showed that, for all three experimental tests, the thermal efficiency of the VTSC would increase by enhancing the average solar radiation.

1. INTRODUCTION

Solar water heaters are widely employed around the world, and their evacuated tube type is among the most popular due to their plainness and superior performance compared to flat-plate collectors, particularly in harsh weather. The water-in-glass design is more common than other types of VTSCs due to its lower cost and easier manufacturing and installation procedures. Another design applies a heat-pipe device with a mediator to transfer heat from the heating components to the tank [1]. Thus, the working fluid faces a phase change phenomenon and moves up and down. Water-in-glass tube-based collector glass tubes joined to a tank or shell. Each tube is restricted by a larger-diameter second glass tube. The ring-shaped room between the tubes is evacuated to reduce heat loss. The working fluid, commonly water, moves from the tank to the tubes, receives heat, and then returns through a natural circulation mechanism to the tank [2]. Yi-Hsuan Hung et al. assessed the thermal performance of a heat pipe by alumina-based nanofluids. A discussion was presented on the impacts of the tilt angle (10°, 40°, 70° and 90°), heat pipe length, working fluid's charged volume ratios (20 %, 40 %, 60 % and 80 %), heating power (20 W, 30 W, and 40 W), and nanoparticles' weight fraction on the total thermal conductivity of the heat pipe to assess the thermal performance. At 40 W heating power, the optimum thermal performance was 22.7 %, 56.3 %, and 35.1 %, respectively, for Al_2O_3/water nanofluid heat pipes of 0.3 m, 0.45 m, and 0.6 m, which was superior to that for pipes applying deionized water[2] as the working fluid [3]. Several studies have characterized the total performance of water-in-glass evacuated tube collectors; the total efficiency was in the range of 50 to 60 % [4-6]. Progressive numerical methods may evaluate the performance and find probable procedures to modify evacuated tubes' designs [7]. A heat-pipe based collector has an equivalent set of tubes joined to a tank. Each tube is made of a finned copper pipe (heat pipe) enclosed to a glass tube, and the annular space is evacuated. The heat pipe is a closed utensil with a capillary wick structure and a little vaporizable fluid. It is on the basis of an evaporating-condensing cycle with an evaporation stage using the solar heat accompanied by a condensation stage where the heat is discharged to the heat sink or metal plate over the tube or connect to the tank-tubes. Through natural circulation, the working fluid moves between the two stages to transfer the heat [8-9]. Assessment of the total yield of solar collectors is performed by using proven ways based on international criteria [10-12]. Many efforts have been developed to predict the total efficacy in different climates. Various studies have evaluated the thermal performance of evacuated-tube solar collectors and compared them with their level plate correlates [13]. Evacuated-tube collectors are produced in determined sizes and mounted inclined at an angle, to be measured by the assumed location latitude. Different factors influence collectors' performance such as weather conditions, the tilt angle, and the dimensions of the collector. The optimal performance is obtained when solar radiation hits the collector elements at a right angle to enhance the mechanism of energy absorption [14]. Zamzamian et al. [15] experimentally investigated the convective heat transfer coefficient of CuO/EG and Al_2O_3/EG nanofluids in the double pipe and plate heat exchangers in turbulent current. There was an enormous increase in the nanofluids' convective heat transfer

*Corresponding Author's Email: mohsenmansouri.87@gmail.com (M. Mansouri)

2. Deionized water (DI water, DIW or de-ionized water), often synonymous with demineralized water/DM water is water that has had almost all of its mineral ions removed, such as cations like sodium, calcium, iron, and copper, and anions such as chloride and sulfate. Distilled or deionized water has been the most common form of purified water mechanically filtered or processed to remove impurities and make it suitable for use.

coefficient from 2 % to 50 % in comparison with the base fluid. The nanofluid's convective heat transfer coefficient raised with an increase in nanofluid temperature and nanoparticles' concentration. Results depicted that homogenously stabilized and dispersed nanoparticles enhanced the exerted convective heat transfer coefficient of the base fluid significantly. The greatest and lowest enhancements in experiments were 49 % and 3 %, respectively. Jamal-Abad et al. studied the heat transfer coefficient and friction factor of the Al–water and Cu–water nanofluids flowing in a spiral coil in the laminar flow regime. They found that the Nusselt number increased by enhancing De number and nanofluids concentration. Nusselt number oscillations may be detected for various nanofluids induced by the secondary flow [16]. In another study, the impact of nanoparticles on the solar flat-plate collector efficiency was examined. A direct synthesis procedure was used to provide Cu–water nanofluid to be applied as working fluid in a solar collector. ASHRAE 93 standard was used to evaluate the solar collector. The collector efficiency was higher when the concentration of nanoparticles increased, and the efficacy of collector at 0.05 wt % was approximately 24 % higher than that of the pure base fluids for the given conditions. Hence, authors suggested that nanofluids could be used in solar collectors [17]. A study investigated the impact of Cu nanoparticle on the efficacy of a flat-plate solar collector. The weight fractions of the nanoparticles with a diameter of 10 nm were 0.2 % and 0.3 % of the nanofluid. A one-stage procedure prepared copper nanofluid by reducing $CuSO_4.5H_2O$ with $NaH_2PO_2.H_2O$ in ethylene glycol. Various volume flow rates of the nanofluid from 0.016 to 0.050 kg/s were used to conduct the experiments, and the ASHRAE 93 standard evaluated the solar collector's performance. By elevating the weight fraction of nanoparticle, the collector efficacy improved. Moreover, the least eliminated energy parameter may be obtained via 0.3 wt % Cu/ EG nanofluid at 1.5 lit/min, and the maximum parameter of absorbed energy was obtained under equivalent conditions [18]. This research aims to evaluate experimentally the thermal performance of glass vacuum tube solar collectors (VTSC) by using alumina nanofluids as the working fluid compared to the deionized water base fluid. Besides, the effect of changing in solar radiation and nanoparticle weight concertation will be assessed.

2. MATERIALS AND METHOD

The efficiency of a collector expresses how it works in the long term. There are some standards, such as ASHRAE 93, ISO 9806-1, and EN12975-2, for finding the performance of solar collectors. Despite the slight difference between these standards, they are all appropriate for calculating the collector efficiency. These standards have been used for many years in solar energy and demonstrated a high accuracy.

2.1. Experimental setup

Standard cycle based on ASHRAE 93 and the variables are displayed in Figure 1. Environmental conditions such as temperature, humidity ratio, and wind speed can be obtained using some certain sensors. Furthermore, the specific environmental conditions and steady-state conditions that should be considered and kept during the experiments are listed in Tables 1 and 2, respectively. Figure 2 depicts the whole system with a standard water-in-glass collector made of 15 evacuated tubes that have been used in the so-called setup. The experimental setup is a closed-loop circuit with compulsory parts and evaluation instruments (Figure 1).

Table 1. Environmental conditions required.

Variable	Absolute limits
Total solar irradiance normal to sun (W/m^2)	790 (minimum)
Diffuse fraction (%)	20 (maximum)
Wind speed, u (m/s)	$2.2 < u < 4.5$
Incidence angle modifier	98 % < normal incidence value < 102 %

Table 2. The allowed maximum variation of key variables.

Variable	Maximum variation
Total solar irradiance normal to surface (W/m^2)	±32
Ambient temperature (K)	±1.5
Volume flow rate	The greater of ±2 % or ±0.005 (gpm)
Inlet temperature	The greater of ±2 % or 1 (K)

A centrifugal pump (Figure 3) circulates the working fluid through the storage tank and the collector. It possesses pipe connections: two located near the top of the tank and two close to the bottom. To utilize stratification of storage tank, pipes supplying the collector array and the cold-water inlet have to join the bottom ports, and the pipes which return to the tank from the collector array and hot water supplied to the load are required to be connected to near the top ports. Openings of instrumentation are required in addition to openings for drains, relief valves, and the like.

2.2. Measurement tools

Solar power meter, three thermometers, anemometer, and water flow meter were used to measure solar radiation, fluid and ambient temperature, wind speed, and flow rate.

2.3. Describing the test device

The solar collector efficiency was evaluated in this test according to the ASHRAE93 standard method. In this method, a collection of devices creating a cycle was used. In this test, the rate of solar radiation was measured by TES 1333R Datalogging. The input and output temperature of the fluid was measured by thermometer PT-100, and the data was recorded on the monitor of Novel Solar Technologies Laboratory. Therefore, the ambient temperature was measured by a portable thermometer, and a flow meter was embedded in the system to estimate the fluid flow discharge. A differential temperature sensor or controller measuring the outlet and inlet temperatures of the collector (PT-100) regulates the system flow by switching the circulation pump on when the storage tank temperature is lower compared with that of the collector. An air vent over the collector makes air released to the system. Drain valves are set under the storage tank to evacuate and fill the circuit when needed. The piping network is coated by a polyurethane foam layer to reduce heat loss. A digital flow meter was set in the circuit to estimate the rate of flow inside the system. Finally, the solar radiation was estimated by a pyranometer TES 1333R Datalogging, connected to a data logger (Figure 4).

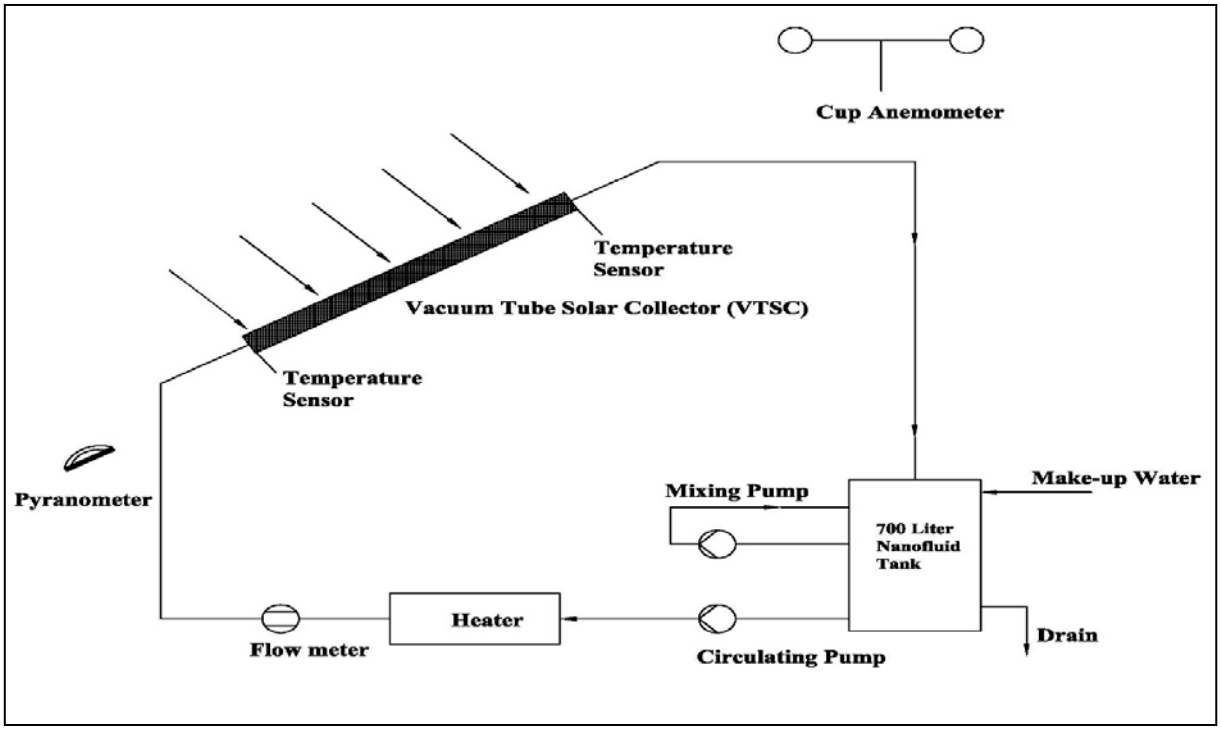

Figure 1. Experimental setup schematic of the system.

Figure 2. Evacuated tube using in this setup.

Figure 3. A view of centrifugal pump.

Figure 4. Pyranometer TES 1333R.

3. NANOFLUID PREPARATION

The nanofluids used in this study were produced by a two-step method in Novel Solar Technologies Laboratory at Materials and Energy Research Center. Thus, after weighing the Al_2O_3 nanoparticles made by MK-nano company, Canada (with a diameter of 15 nm using the digital scale with 0.011 gr accuracy), they were mixed in water. Then, the SDBS surfactant was added to the mixture and the suspension was placed on a magnetic mixer for a certain time to disperse the particles inside the base fluid uniformly. Table 3 indicates the time duration for each step of the nanofluids' production process. As can be observed, the time duration for each step rises with the augmentation of the nanofluid mass percentage.

Table 3. The time duration for each step in nanofluids production process.

Nanofluid type	Magnetic mixing (min)	Ultrasonic (min)
0.5 mass percent	130	80
1 mass percent	150	120

To obtain the required mass of nanoparticles for producing the nanofluid with aimed mass percentage ($\phi_{m)}$, Equation 1 was used.

$$\varphi_m = \frac{m_p}{m_w + m_p} \times 100 \quad (1)$$

For example, 10.1 gram of Al_2O_3 nanoparticles generated 1 liter of Al_2O_3-water nanofluid with 1 % mass percentage. Figure 5 depicts the TEM image of the applied nanoparticles. The mixture was then stabilized under a continuous sonication using an ultrasound vibrator (Hielscher, UP400S, 400 Watt, 24 kHz) (Figure 6). The ultrasonic process time is divided into three time periods of 20 min. To examine the stability of nanofluids, the density of the nanofluid at various locations and times during the course of the experiment was measured. For the duration of the experiment, no significant changes in the density and sedimentation were observed. The pH of the solution was measured after adding the surfactant (pH of the pure water was measured equal to 6.41) (Table 4).

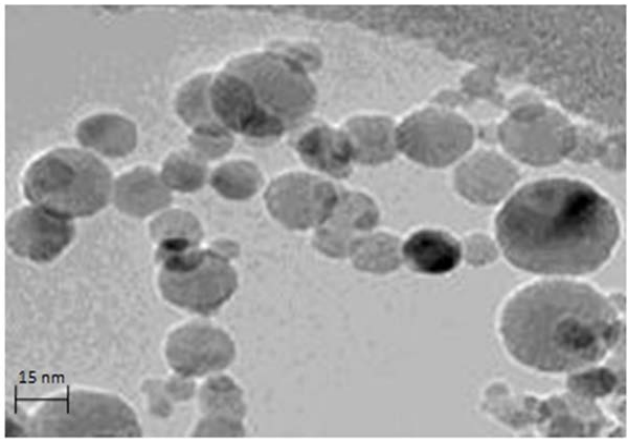

Figure 5. TEM image of Alumina nanoparticles.

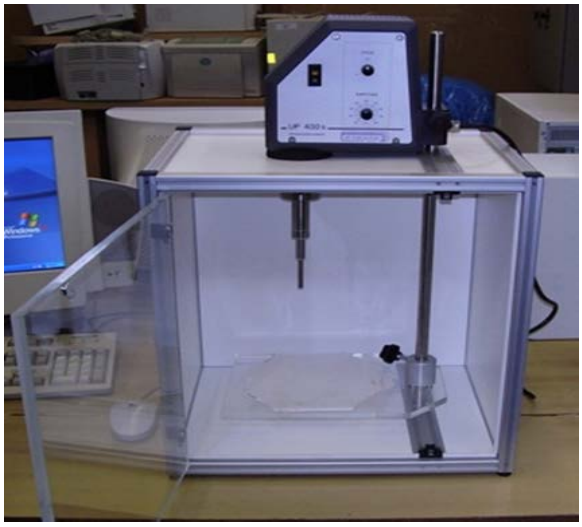

Figure 6. A view of Hielscher ultrasonic device.

Table 4. The results of pH related to the produced nanofluids.

Type of nanofluid	pH of surface activator	pH of nanofluid
0.5 mass percent	6.69	7.66
1 mass percent	6.81	7.3

For this purpose, the Sonotrode H22 probe with a diameter of 22 mm was used for applying the ultrasonic waves to the solutions with 100 to 2000 ml. During the stabilization of nanofluid inside the ultrasonic device, Al_2O_3 dry nanoparticles were dispersed ultrasonically in a cold water bath to prevent overheating of the base fluid. In addition, a specific cover was put in the container to hinder the base fluid evaporation.

4. THE THEORY OF THE TEST

The following different factors affect the effectiveness of a solar collector:

1. Scattered solar radiation
2. Direct solar radiation
3. Weather conditions (wind, rain, snow, etc.)
4. Heat dissipation (by displacement mechanism)
5. Heat dissipation (by thermal conductivity mechanism)
6. Absorbing the thermal radiation
7. The thermal radiation of the collector glass
8. Collector reflection

The amount of energy absorbed by the collector to collector surface under stable conditions equals the useful energy transferred to the fluid and the amount of energy dissipated to the collector surface according to Eq. 2.

$$\dot{Q}_{abs} = \dot{Q}_u + \dot{Q}_L \quad (2)$$

$$\dot{Q}_u = \dot{m} C_f (T_{f_o} - T_{f_i}) \quad (3)$$

$$\eta_i = \frac{\dot{Q}_u}{A_C I(t)} \quad (4)$$

$\dot{Q}_{abs}$, $\dot{Q}_u$, and $\dot{Q}_L$ are the energy absorbed by the collector, useful energy, and lost energy, respectively. $\dot{m}$, C_f, T_{f_i}, T_{f_o}, $I(t)$, and A_C are fluid flow discharge in the collector, fluid thermal capacity, input and output temperature of fluid to the collector, solar radiation rate, and the collector surface, respectively. Heat dissipation from the collector to the ambient occurs via the collector glass, body, and bottom. This dissipation occurs through conductivity, displacement, and radiation. In this test, the amount of heat transfer from the collector upper surface was studied. In the initial step of the test, the base fluid (water) was tested by the mentioned method by ASHARE 93 standard with respect to the following assumptions:

$$C_{bf} = 4200 \ {}^{j}/_{Kg\,K} \quad (5)$$

By assuming that water density equals $1000 \ {}^{kg}/_{m^3}$:

$$\dot{m} = 1 \ {}^{lit}/_{min} = 0.16667 \ {}^{Kg}/_{sec} \quad (6)$$

$$\Delta t = 15 \text{ min} \quad (7)$$

5. UNCERTAINTY ANALYSES

Table 5 shows the uncertainties of the mass flow rate, temperature, solar irradiation, and wind speed within the experiments. The following equation is applied to evaluate errors of the dependent items [19].

$$\psi_c(y) = \sqrt{\sum_{i=1}^{n} \psi(x_i)^2 . (\frac{\partial y}{\partial x_i})^2} \quad (8)$$

Table 5. Independent uncertainties.

Variable	Quantity	Unit	Uncertainty	Conf. (%)
Mass flow	1	Kg/s	±5 %	95
Temperature	2	^oC	0.1 ^oC	95
Solar irradiance	1	W/m^2	±32	95
Wind speed	1	m/s	±5 %	95

In this correlation, xi and y represent independent and dependent variables, respectively. Equation 9 depicts the relationship between Equations 6 and 8 to evaluate the uncertainty of thermal efficiency. The uncertainties result from the inaccuracy of the thermocouples, flowmeter, pyranometer, and anemometer. Therefore, appropriate care was exercised to minimize errors within the tests.

$$\psi(\eta) = \psi(\dot{m})^2 . (\frac{\partial \eta}{\partial \dot{m}})^2 + \psi(T)^2 . (\frac{\partial \eta}{\partial T})^2 + \psi(G)^2 . (\frac{\partial \eta}{\partial G})^2 \quad (9)$$

6. RESULTS AND DISCUSSION

Solar energy radiations for the first step of experiment measured by the pyranometer are given in Table 6.

Table 6. Information data for the first step (C_p=4200 kj/Kg.K, $\dot{m}$=0.016667 Kg/s).

T_i (^oC)	T_o (^oC)	T_a (^oC)	Q (Lit/s)	I_t (W/m^2)	η_i
29.4	29.5	29	1	790	0.141095
29.3	29.4	29	1	814	0.136935
26.9	27	29.4	1	842	0.132381
27.6	27.7	29	1	875	0.127389
29.4	29.6	29	1	924	0.241266
30	30.2	29.4	1	917	0.243108
30.3	30.4	30	1	935	0.119214
30.5	30.6	30	1	940	0.11858
29.9	30	30	1	910	0.122489

This step of the test was conducted on June 23, 2012. The tests were based on ASHARE93 standard at an interval of symmetry compared to the solar noon (13:07). The most important variable for studying the solar collector performance is its efficiency, indicating the useful energy rate. The collector efficiency for different radiations is depicted in Figure 7. The mean collector efficiency for base fluid, i.e., water, was about 14.5 %. If the diagram of collector efficiency in terms of average solar radiation is drawn, it will be as follows. The average efficiency of the collector was determined to be15.4 % when water was used as working fluid. The changes in the collector efficiency with the ambient temperature are illustrated in Figure 8. Firstly, the collector efficiency increases with the increment of ambient temperature. The efficiency reaches its maximum value at 29.4 ºC.

The collector efficiency decreases with the temperature enhancement of more than 29.4 ºC. Because by assuming the ASHRAE 93 standard, an attempt has been made to keep the input temperature to the collector (T_i) constant during the test. On the basis of the following equation, the equation's second term rises with the temperature increment (Ta). Based on T_i value, this fraction gets small and, then, large, thus affecting the efficiency.

$$\eta = F_R \tau\alpha - F_R U_L \left(\frac{T_i - T_a}{G_t}\right) \quad (10)$$

This test is not indicated in the ASHRAE 93 standard process, yet is beneficial for expressing the solar collector performance. Obviously, the variation between the output and input temperature decreases with the elevation of the input temperature causing a reduction in the collector efficiency.

The decreasing trend of efficiency with the inlet temperature augmentation is completely obvious in Figure 9. Based on the vacuum tube collector efficiency equation, it can be simply found by Eq. (10).

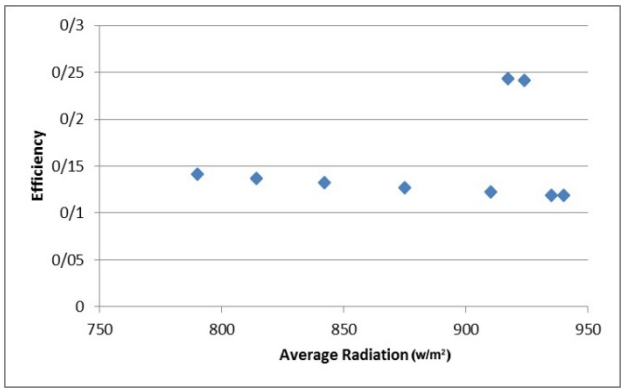

Figure 7. Diagram of collector efficiency for water according to average solar irradiation.

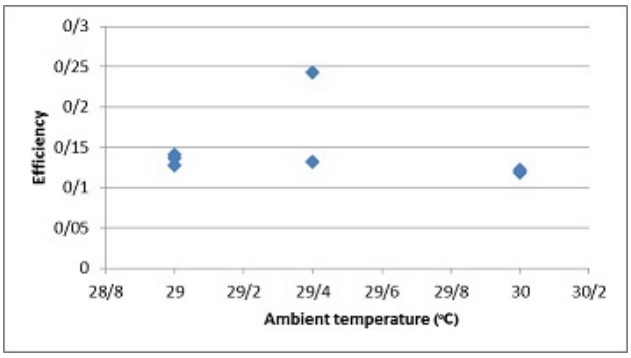

$$\eta = F_R\tau\alpha - F_R U_L \left(\frac{T_i - T_a}{G_t}\right)$$

Figure 8. Variation of collector efficiency for water with ambient temperature.

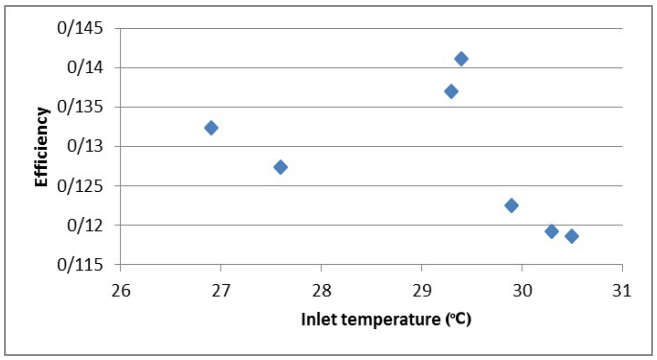

Figure 9. Variation of collector efficiency for water with inlet temperature.

Efficiency-variable diagram $x = \frac{T_i - T_a}{G_t}$ is the most useful diagram for expressing the VTSC efficiency. When the radiation and flow intensity are constant, variables F_R,τα, and $U_L$are almost constant. This diagram is a direct line with a negative slope for obtaining $F_R\tau\alpha$ and $-F_R U_L$values. This is not true for different conditions of temperature, ambient, and radiation intensity, and a direct line diagram should be matched for the data. The horizontal axis collides in η=0. This situation occurs when the solar radiation rate is the least or the collector's fluid input temperature is very high. These conditions are called stagnation conditions and occur when there is no fluid flow. Figure 10 shows this curve. The direct line with equation y=-3.9024x+0.121 is the most appropriate line for the current data obtained by EXCEL software. In this equation, x is $(T_i-T_a)/G_t$ as the horizontal axis.

Table 7. Characteristics of tested collector.

Line equation	y=-3.9024x+0.121
$F_R\tau\alpha$	0.121
$-F_R U_L$	-3.9024

By using this line equation, the solar collector variables can be obtained as shown in Table 7. Thus,

$$\frac{U_L}{\tau\alpha} = 32.25 \qquad (11)$$

In the second step, the test for alumina-water nanofluid with a mass concentration of 0.5 % was conducted the same as the previous step with specific heat calculated by Eq. 9:

$$C_{pnf} = \frac{\phi.\left(\rho_{np}.C_{pnp}\right) + (1-\phi).\left(\rho_f.C_{pf}\right)}{\rho_{nf}} \qquad (12)$$

$$C_{nf} = 4165.49\ {}^{j}/_{Kg\,K} \qquad (13)$$

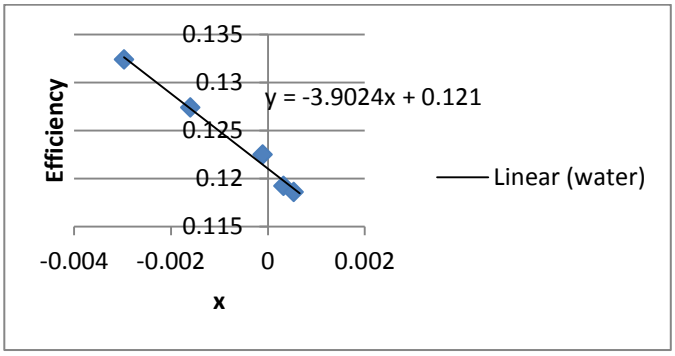

Figure 10. Collector efficiency for water according to x value.

Table 8. Second step data (C_p=4200 kj/Kg.K, ṁ=0.016667 Kg/s).

T_i (°C)	T_o(°C)	T_a(°C)	Q $(\frac{lit}{s})$	$I_t(\frac{W}{m^2})$	η_i
29	29.1	29	1	884	0.1255
29.6	29.9	29.5	1	840	0.3964
31.5	31.7	31.5	1	940	0.2361
31.9	32.1	31.5	1	970	0.2288
32.3	32.4	32	1	957	0.1159
32.3	32.6	32	1	950	0.3505
32.3	32.6	32	1	936	0.3557
32.4	32.6	32	1	900	0.2466
29	29.1	29	1	884	0.1255

This step of the test was conducted on June 25, 2012. The tests were based on ASHARE93 standard at an interval of symmetry than the solar noon (13:08) on day. The collector efficiency is shown in Figure 11 according to average solar radiation for Al_2O_3 nanofluid based on water with a mass concentration of 0.5 %. This figure clearly shows that the collector efficiency in radiation 970-840 w/m^2 has almost a

constant trend, and there will be a less increase in radiation more than 900 w/m^2. The average efficiency of the collector in this condition will be about 25.7 %, which is more than the collector efficiency value for the base fluid.

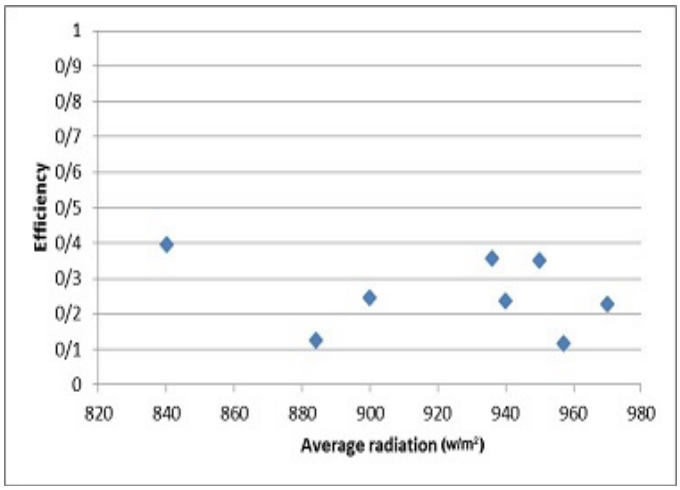

Figure 11. Collector efficiency for 0.5 wt. % Al_2O_3/water nanofluid according to average solar irradiation.

In the second step, the test was conducted for Al_2O_3nanofluid based on water with a mass concentration of 1 % as the previous step with the following specific heat calculated by Eq. 9:

$$C_{nf} = 4148.98\ {}^{j}/_{Kg\ K} \quad (14)$$

Table 9. Third step data (C_p=4200 kj/Kg.K, ṁ=0.016667 Kg/s).

T_i (°C)	T_o(°C)	T_a(°C)	Q ($\frac{lit}{s}$)	I_t($\frac{W}{m^2}$)	η_i
29	29.1	29	1	874	0.1264
29.6	29.9	29.5	1	835	0.3971
31.5	31.7	31.5	1	930	0.2377
31.9	32.1	31.5	1	965	0.2291
32.3	32.5	32	1	950	0.2327
32.3	32.6	32	1	943	0.3517
32.3	32.6	32	1	930	0.3566

This step of the test was conducted on June 27, 2012. The tests were based on ASHARE93 standard at an interval of symmetry than the solar noon (13:09) on day. The collector efficiency in terms of average solar radiation for Al_2O_3 nanofluid based on water with a mass concentration of 1 % is shown in Figure 12. In this figure, the radiation ranged from 835 to 965 w/m^2. Firstly, the significant radiation of collector efficiency is observed with the increase of average radiation. After the radiation reaches 884, the efficiency increases and, then, remains constant.

Table 10. Average collector efficiency for employed working fluids.

Working fluid type	Average collector efficiency (%)
Water	15.3
0.5 wt. % nanofluid	25.7
1 wt. % nanofluid	27.2

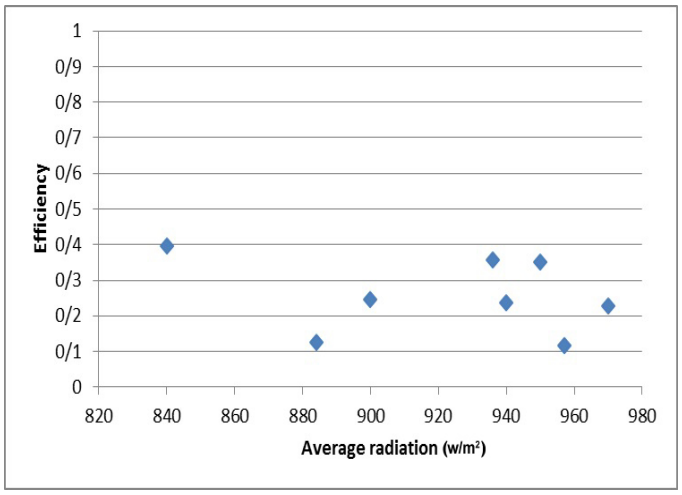

Figure 12. Diagram of collector efficiency for 1 wt. % Al_2O_3/water nanofluid according to average irradiation.

Thus, the mean solar collector efficiency for the nanofluid with a mass concentration of 1 % is about 27.2 %. This is while the maximum efficiency rate in this mass percentage is 39.7 %, which is the maximum efficiency during the test, which was more than the values of the last two steps. Table 10 indicates a summary of the results conducted in three steps. The changes of VTSC efficiency with time are illustrated in Figure 13. The horizontal axis shows the time. The data are drawn for the symmetrical time interval of 1.5 hours related to the solar noon. In all three tests, the collector effectiveness augmented through approaching the solar noon while it decreased after reaching the solar noon. Such an increase in nanofluids was observed with more delay than the base fluid. Additionally, the efficiency of the collector for nanofluid samples was more than the base fluid at all hours, which may reduce the desired level for transferring the heat in collectors. The costs related to these devices can be decreased using nanofluid spontaneously, causing a reduction in the initial costs.

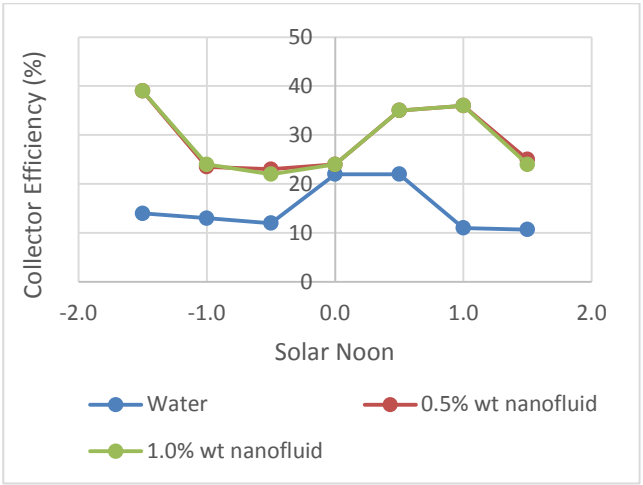

Figure 13. Variation of vacuum tube collector efficiency with time.

Figure 14 shows the collector efficacy for different concentrations of nanoparticles.

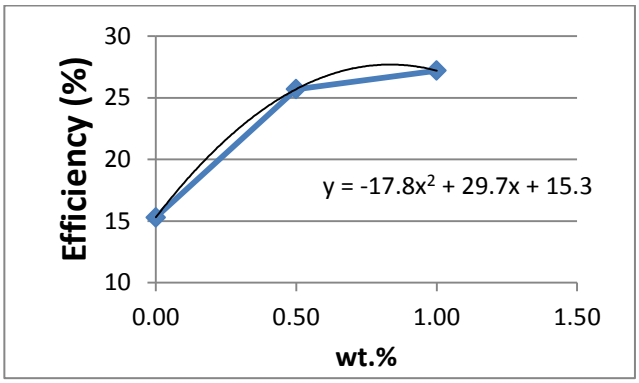

Figure 14. Variation of vacuum tube solar collector efficiency with nanofluid concentration.

The figure clearly shows that the collector efficiency has an ascending trend with the augmentation of nanofluid concentration and reaches from 15.3 % for base fluid to 27.2 % for 1 % nanofluid. Figure 15 shows the maximum values related to the nanofluid with a mass concentration of 1 % and then 0.5 %. The collector efficiency experienced more fluctuations when the nanofluid was used.

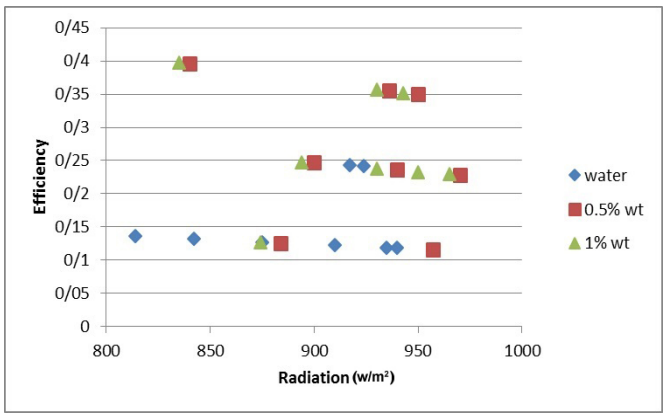

Figure 15. Trend of vacuum tube solar collector efficiency changes with average solar radiation.

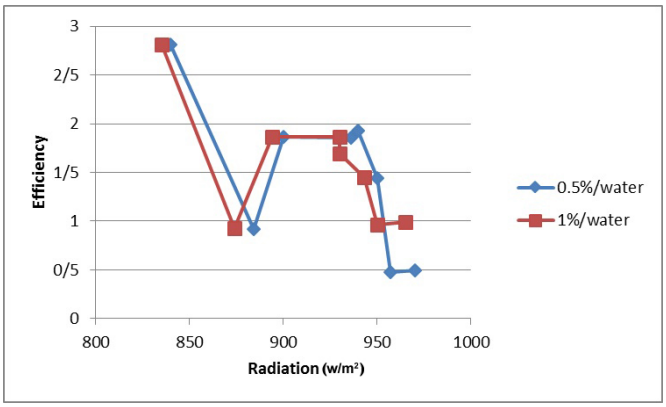

Figure 16. Diagram for the ratio of solar collector efficiency with average solar radiation.

Figure 16 depicts the diagram for the ratio of solar collector efficiency changes (efficiency using nanofluid/efficiency using water) to the average received radiation.

7. CONCLUSIONS

In general, if the variation figure of the collector average efficiency in different radiations is drawn based on mass percentage changes, the collector efficiency will rise with the increment of nanoparticle mass percent. Using nanofluids as a new working fluid in the VTSC for heat transfer can significantly affect the heat transfer rate elevation.

This phenomenon was examined in this research for a VTSC by applying the Al_2O_3-water nanofluid. The results indicated that the VTSC efficiency could significantly increase by employing this nanofluid. In general, for 0.5 % and 1 % nanofluids, the efficiency increased to 67.9 % and 77.7 % compared to water as working fluid. In other words, nanoparticles in fluid led to the absorption of energy fluid through the absorbent tube on the collector. If the collector efficiency changes are drawn in a diagram, an increase will be observed in the efficiency of collector by adding the nanoparticles to the base fluid. The efficiency trend changed with average solar radiation for all three samples (Figure 15). The diagrams indicated some interesting results as other advantages of using nanofluids in solar collector. In both samples, i.e., the nanofluids with 1 % and 0.5 % mass concentrations, collector efficiency ratio declined with the enhancement of the average solar radiation. In fact, the nanofluids in less radiation increased more efficiently. One of the disadvantages of solar collectors is their low efficiency in low radiations far from the solar noon. Therefore, the system can be set up quickly when employing the nanofluids, which is considered as a notable advantage.

8. ACKNOWLEDGEMENT

The authors would like to specially thank the financial support from Materials and Energy Research Center (MERC) to carry out this research project.

NOMENCLATURE

A_c	Collector surface (m^2)
C_p	Specific heat at constant pressure (J/kg.K)
F_R	Collector heat removal factor
G_t	Total solar incident radiaton (W/m^2)
I_t	Incident solar irradiation (W/m^2)
$\dot{m}$	Mass flow rate (kg/s)
Q	Volume flow rate (lit/s)
$\dot{Q}_u$	Useful gain of energy(W)
$\dot{Q}_L$	Lost energy (W)
T	Temperature (K)
U_L	Loss coefficient ($W/m^2.K$)
x	Reduced temperature, independent variable
y	Dependent variable
Greek letter	
η	Collector performance efficiency (%)
ρ	Density (kg/m^3)
$\tau\alpha$	Transmission- absorption coefficient
φ	Volume fraction
φ_m	Mass percent
ψ	Error of independent variables
Subscripts	
a	Ambient
abs	Absorbed
bf	Basefluid
f	Fluid
i	Inlet
nf	Nanofluid
o	Outlet
p	Particle
np	Nanoparticle
W	Deionized water

REFERENCES

1. Kalogirou, S.A, "Solar thermal collectors and applications", ***Progress in Energy and Combustion Science***, Vol. 30, (2004), 231-295. (https://doi.org/10.1016/j.pecs.2004.02.001).
2. Morrison, G.L., Budihardjo, I. and Behnia, M., "Water-in-glass evacuated tube solar water heaters', ***Solar Energy***, Vol. 76, (2004), 135-140. (https://doi.org/10.1016/j.solener.2003.07.024).
3. Hung, Y.-H., Teng, T.-P. and Lin, B.-G., "Evaluation of the thermal performance of a heat pipe using alumina nanofluids", ***Experimental Thermal and Fluid Science***, Vol. 44, (2013), 504-511. (https://doi.org/10.1016/j.expthermflusci.2012.08.012).
4. Morrison, G.L., Budihardjo, I. and Behnia, M., "Measurement and simulation of flow rate in a water-in-glass evacuated tube solarwater heater", ***Solar Energy***, Vol. 78, (2005), 257-267. (https://doi.org/10.1016/j.solener.2004.09.005).
5. Kim, Y. and Seo, T., "Thermal performance comparisons of the glass evacuated tube solar collectors with shapes of absorber tube", ***Renewable Energy***, Vol. 32, (2007), 772-795. (https://10.1016/j.egypro.2011.05.071).
6. Zhang, X.R. and Yamaguchi, H., "An experimental study on evacuated tube solar collector using supercritical CO_2", ***Applied Thermal Engineering***, Vol. 28, (2008), 1225-1233. (https://doi.org/10.1016/j.applthermaleng.2007.07.013).
7. Hayek, M., "Investigation of evacuated-tube solar collector's performance using computational fluid dynamics", ***Proceedings of ACTEA09***, (2009), 240-244. (https://doi.org/ 10.1109/ACTEA.2009.5227901).
8. Walker, A., Mahjouri, F. and Stiteler, R., "Evacuated-tube heat-pipe solar collectors applied to the recirculation loop in a federal building", ***NREL/CP***-710-36149, (2004). (https://doi.org/ 10.1115/isec2004-65132).
9. Kim, Y. and Seo, T., "Thermal performances comparisons of the glass evacuated tube solar collectors with shapes of absorber tube", ***Renewable Energy***, Vol. 32, (2007), 772–795. (https://doi.org/10.1016/j.renene.2006.03.016).
10. "Methods of testing to determine the thermal performance of solar collectors", ***ASHRAE Standard 93***, Atlanta, GA, USA, (2003). (https://doi.org/10.3403/00094097).
11. Hill, J.E. and Streed, E.R, "A method of testing for rating solar collectors based on thermal performance", ***Solar Energy***, Vol. 18, (1976), 421-429. (https://doi.org/10.1016/0038-092X(76)90008-6).
12. Proctor, D., "A generalized method for testing all glasses of solar collectors, II: Evaluation of collector thermal constants", ***Solar Energy***, Vol. 32, (1984), 387-394. (https://doi.org/10.1016/0038-092x(84)90283-4).
13. Zambolin, E. and Del Col, D., "Experimental analysis of thermal performance of flat plate and evacuated tube solar collectors instationary standard and daily conditions", ***Solar Energy***, Vol. 84, (2010), 1382-1396. (https://doi.org/10.1016/j.solener. 2010.04.020).
14. Tang, R., Gao, W., Yu, Y. and Chen, H., "Optimal tilt-angles of all-glass evacuated tube solar collectors", ***Energy***, Vol. 34, (2009), 1387-1395. (https://doi.org/10.1016/j.energy.2009. 06.014).
15. Zamzamian, S.A.H., Nasseri Oskouie, S., Doosthoseini, A., Joneidi, A. and Pazouki, M., "Experimental investigation of forced convective heat transfer coefficient in nanofluids of Al_2O_3/EG and CuO/EG in a double pipe and plate heat exchangers under turbulent flow", ***Experimental Thermal and Fluid Science***, Vol. 35, (2011), 495-502. (https://doi.org/ 10.1016/j.expthermflusci.2010.11.013).
16. Jamal-Abad, M.T., Zamzamian, S.A.H. and Dehghan, M. ,"Experimental studies on the heat transfer and pressure drop characteristics of Cu–water and Al–water nanofluids in a spiral coil" ***Experimental Thermal and Fluid Science***, Vol. 47, (2013), 206-212. (https://doi.org/10.1016/j.expthermflusci.2013. 02.001).
17. Jamal-Abad, M.T., Zamzamian, S.A.H., Imani, E. and Mansouri, M., "Experimental study of the performance of a flat-plate collector using Cu–water nanofluid", ***Journal of Thermophysics and Heat Transfer***, Vol. 27, No. 4, (2013), 756-760. (https://doi.org/10.2514/1.t4074).
18. Zamzamian, S.A.H., Keyanpour Rad, M., Kiani Neyestani, M. and Jamal-Abad, M.T., "An experimental study on the effect of Cu-synthesized/EG nanofluid on the efficiency of flat-plate solar collectors", ***Renewable Energy***, Vol. 71, (2014), 658-664. (https://doi.org/10.1016/j.renene.2014.06.003).
19. Jamal-Abad, M.T., Saedodin, S. and Aminy, M., "Experimental investigation on a solar parabolic trough collector for absorber tube filled with porous media", ***Renewable Energy***, Vol. 107, (2017), 156-163. (https://doi.org/10.1016/j.renene.2017.02.004).